Accepted Manuscript
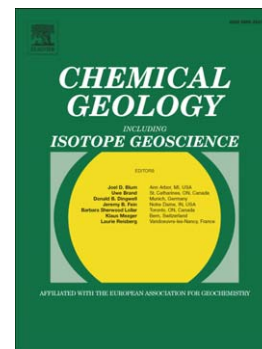
Novel 1*H*-Pyrrole-2,5-dione (maleimide) proxies for the assessment of photic zone euxinia

Sebastian Naeher, Kliti Grice

Please cite this article as: Naeher, Sebastian, Grice, Kliti, Novel 1*H*-Pyrrole-2,5-dione (maleimide) proxies for the assessment of photic zone euxinia, *Chemical Geology* (2015), doi: 10.1016/j.chemgeo.2015.03.020

Novel 1*H*-Pyrrole-2,5-dione (maleimide) proxies for the assessment of photic zone euxinia

Sebastian Naeher [*] and Kliti Grice [*]

Western Australia Organic and Isotope Geochemistry Centre (WA-OIGC), Department of Chemistry, The Institute for Geoscience Research, Curtin University, GPO Box U1987, Perth, WA 6845, Australia

* Corresponding authors. Tel.: +61 8 9266 2474.

E-mail addresses: Sebastian.Naeher@curtin.edu.au (S. Naeher); K.Grice@curtin.edu.au (K. Grice)

ABSTRACT

1H-Pyrrole-2,5-diones (maleimides) and 1-alkyl-2,3,6-trimethylbenzenes (aryl isoprenoids), degradation products of tetrapyrrole pigments and carotenoids respectively, were analysed and compared with pristane/phytane (Pr/Ph) ratios to reconstruct past redox conditions in three geologic sections. One section comes from the Middle-Late Devonian and was deposited before the Frasnian-Famennian boundary mass extinction. The two other sections span the Late Permian to the Early Triassic as well as the Late Triassic to the Early Jurassic, and recorded the Permian-Triassic (P/T) and Triassic-Jurassic (T/J) extinction events respectively. The 2-methyl-3-*iso*-butyl-maleimide (Me,*i*-Bu maleimide) to 2-methyl-3-ethyl-maleimide (Me,Et maleimide) and 2-methyl-3-*n*-propyl-maleimide (Me,*n*-Pr maleimide) to Me,Et maleimide ratios (Me,*i*-Bu/Me,Et and Me,*n*-Pr/Me,Et ratios) in the studied sections revealed a moderate to strong negative correlation to the aryl isoprenoid ratio (AIR), defined as (C_{13}–C_{17} 1-alkyl-2,3,6-trimethylbenzenes)/ (C_{18}–C_{22} 1-alkyl-2,3,6-trimethylbenzenes), indicating that these maleimide ratios can be used as robust, specific indicators of photic zone euxinia (PZE). These results agreed with Pr/Ph ratios, which were used as diagnostic indicators to differentiate between oxic and anoxic conditions. In agreement with previous studies, the novel maleimide proxies suggest that all three mass extinctions were largely characterised by PZE depositional conditions.

2

1. Introduction

Oxygen depletion in aquatic systems is a common phenomenon throughout Earth's history. Today, it has increasingly been recognised that oxygen concentrations decrease in various aquatic environments worldwide (e.g. open oceans, coastal areas, lakes, fjords, lagoons and embayments) as a result of natural and anthropogenic factors, most notably due to climate change and eutrophication (e.g. Diaz and Rosenberg, 2008; Friedrich et al., 2014). Higher temperatures due to a warming climate reduce the solubility of oxygen and lead to enhanced thermal stratification, which reduces water column mixing associated with a decreasing supply of oxygen to the deeper waters (e.g. Diaz and Rosenberg, 2008; Friedrich et al., 2014). Another factor is eutrophication, which results from the increased supply of nutrients from agriculture, industry and urbanisation. Nutrient supply can lead to high productivity, persistent algal blooms and enhanced organic matter (OM) accumulation and mineralisation, resulting in a decline of deep-water oxygen concentrations (e.g. Middelburg and Levin, 2009). Episodic, periodic or permanent declines in oxygen levels can cause reduced species numbers, decreased biodiversity, or mass mortality events with potentially irreversible extinction of species and the spreading of so called dead zones (e.g. Diaz and Rosenberg, 2008; Friedrich et al., 2014).

Five major extinction events occurred in the Phanerozoic, near the end of the Ordovician, Devonian, Permian, Triassic and Cretaceous Periods (e.g. Raup and Sepkoski, 1982; Barnosky et al., 2011). Various reasons for these extinctions have been proposed, including bolide impacts, climatic changes, volcanism, tectonics, uplifting and weathering processes of mountain ranges and marine transgression and regression cycles (e.g. Hallam and Wignall, 1997; Twitchett, 2006; Barnosky et al., 2011). However, increased water body stratification and related widespread deep-water anoxia (<10 μM O_2), euxinia (free H_2S) as well as ocean acidification may be primary factors in some of the major extinction events (Grice et al., 2005b; Cao et al., 2009; Nabbefeld et al., 2010; Jaraula et al., 2013; Tulipani et al., in press).

Euxinia is an oxygen-depleted state in which free, toxic H_2S is enriched in the water column and may also penetrate into the photic zone to establish PZE, a common phenomenon throughout most of Earth's history (Grice et al., 1996; Brocks et al., 2005; Grice et al., 2005a; Meyer and Kump, 2008; Lyons et al., 2009; Naeher et al., 2013). While seasonal euxinia develops in various modern aquatic ecosystems, persistent euxinic conditions are typically limited to coastal upwelling zones, silled water bodies, fjords and meromictic lakes (e.g. Meyer and Kump, 2008; Friedrich et al., 2014). The primary reason for the development of PZE is increasing algal productivity as the enhanced OM supply to the sediment and associated microbial OM mineralisation processes consume oxygen, causing an overall decline of deep-water oxygen concentrations and increased H_2S production by the reduction of sulfate (e.g. Meyer and Kump, 2008; Friedrich et al., 2014). These processes are often

associated with enhanced nutrient cycling from the sediments, which further facilitate the development of anoxia and euxinia (e.g. Middelburg and Levin, 2009). In coastal environments, the upwelling of nutrient rich waters or the supply of nutrients from major rivers may further enhance oxygen depletion and PZE (e.g. Middelburg and Levin, 2009; Friedrich et al., 2014). Thermal and salinity stratification has the tendency to favour PZE, because a warming climate and distinct sources of saline and fresh waters may lead to reduced mixing (e.g. Meyer and Kump, 2008). Basin morphology can further influence euxinia as an increasing water level in marine basins may create estuarine circulation patterns, which can lead to regional trapping of nutrients (e.g. Meyer and Kump, 2008).

PZE affected water bodies form ideal habitats of specific photosynthetic sulfur bacteria (Chromatiaceae, Chlorobi) (e.g. Pfennig, 1978). These bacteria are capable of anoxygenic photosynthesis, using specific pigments such as tetrapyrroles (e.g. bacteriochlorophylls *a–e*) and carotenoids (okenone, isorenieratene) (Summons and Powell, 1987; Grice et al., 1996; Koopmans et al., 1996; Brocks and Summons, 2003). These pigments and/or their degradation products, such as for instance 1*H*-Pyrrole-2,5-diones (maleimides) and aryl isoprenoids (1-alkyl-2,3,6-trimethylbenzenes), have been used as diagnostic proxies for PZE and, therefore, also oxygen depletion in aquatic environments (e.g. Grice et al., 1996; Brocks and Summons, 2003; Schwark and Frimmel, 2004; Naeher et al., 2013). Here, we test and apply two novel maleimide proxies to three geologic formations which comprise or are close to three major mass extinctions, and compare the data to aryl isoprenoid (AIR)

5

and pristine/phytane (Pr/Ph) ratios for these sites in order to demonstrate the potential of these maleimide indices as specific and robust indicators of PZE in the geologic record.

2. Material and methods

2.1. Study sites

The studied samples (Fig. 1) originate from cores and outcrops previously investigated using lipid biomarkers to characterise major mass extinction events (Grice et al., 2005a; 2005b; Jaraula et al., 2013; Tulipani et al., in press).

The core from the McWhae Ridge (MWR; Canning Basin, Western Australia; S 18°43'40.7'', E 126°4'5.5'', WGS84) was drilled in July 2010 and studied recently by Tulipani et al. (in press). The intersected rock units (Fig. 1a) consist of a faulted reef which drowned in the Early Frasnian (Late Devonian) prior to deposition of marginal slope and basinal facies deposits (Becker et al., 1991; Playford et al., 2009). The studied core section (27.2-42.1 m; Fig. 1a) consists of the interfingering Sadler and Gogo Formations (Tulipani et al., in press): The lower unit (40–42 m depth) comprises latest Givetian-earliest Frasnian age units, consisting of laminated argillaceous shales with thin limestone interbeds and some narrow irregular beds of shelly wackestone and fine grained packstone. In contrast, the upper unit (27–33.5 m depth) is of Frasnian age and consists of finely laminated calcareous shale with few narrow beds of nodular and brecciated micrite as well as fine packstone. The intermediate interval (33.5-40

m), characterised by irregular bedded calcareous siltstone with abundant micrite nodules (37.5-40 m) and argillaceous limestone (33.5-37.5 m), was not studied because of its low organic matter content. The maturity of all samples is low with average T_{max} values (Rock Eval analysis) of <421 °C (Tulipani et al., in press). The core comprises the Late Givetian (Middle Devonian) until the Middle to Late Frasnian (Late Devonian), before the Frasnian-Famennian boundary extinction event (Tulipani et al., in press).

Immature Triassic/Jurassic (T/J) samples from St. Audrie's Bay (SAB; England; N 51°10'54.0'', W 3°17'9.4'', WGS84) are mudstones that were deposited in offshore marine waters from the Upper Rhaetian (Late Triassic) to the Hettangian (Early Jurassic), comprising the Westbury, Lilstock and Blue Lias Formations (Hesselbo et al., 2004; Hounslow et al., 2004; Mander et al., 2008; Jaraula et al., 2013). The outcrop is 63 m high (Fig. 1b) and the section comprises the mass extinction event close to the T/J boundary (Jaraula et al., 2013). The extinction horizon occurs within a short stratigraphic interval from the uppermost Westbury to the lower Lilstock Formation, and the upper Cotham and lower Langport members, which contain almost no benthic macrofossils, have been interpreted as a post-extinction 'Dead Zone' (Mander et al., 2008; Jaraula et al., 2013).

Immature rock samples were obtained from the Hovea-3 borehole in the Perth Basin (PB; Western Australia) as reported by Grice et al. (2005a; 2005b). The cored interval (Fig. 1c) represents the Hovea Member, which is an organic matter enriched zone of the Kockatea Shale (Thomas et al., 2004), deposited in shallow shelf setting below the wave base (Grice et al., 2005a; 2005b). The

base of the core is formed by the Dongara Sandstone, followed by the Inertinitic Interval consisting mainly of fossiliferous black mudstone, sandy siltstone and shelly stormbeds and the Sapropelic Interval, characterised by alternating dark brownish-grey, finely laminated mudstone and thin limestone (Thomas et al., 2004). This section comprises the transition between the Changhsingian (Late Permian) and Griesbachian (Early Triassic) and therefore covers the period of the Permian-Triassic (P/T) mass extinction (Grice et al., 2005a; 2005b). Grice et al. (2005c) suggest that the section is incomplete and contains a hiatus at the P/T boundary on the basis of the rapid shift of biomarker abundances, in particular the high relative abundance of the C_{33} alkylcyclohexane at the onset of the marine ecosystem collapse.

2.2. Lipid biomarker analysis

The detailed procedures used for lipid biomarker analysis are reported in Tulipani et al. (in press), Jaraula et al. (2013) and Grice et al. (2005b). In short, 7–151 g of powdered rock samples were extracted with DCM/MeOH (9:1, v: v) using a Soxhlet apparatus for 48 h (MWR; Tulipani et al., in press) or 72 h (SAB; Jaraula et al., 2013), or using accelerated solvent extraction (PB; Grice et al., 2005b). In all three studies, elemental sulfur was removed using activated copper and total lipid extracts were then separated by silica gel chromatography into six fractions using *n*-hexane for saturated hydrocarbons, *n*-hexane/DCM (8:2, v: v) for aromatic hydrocarbons, *n*-hexane/DCM (1:1, v: v) for nickel porphyrins, DCM for vanadyl porphyrins, DCM/acetone (9.5:1, v: v) for

8

maleimides and DCM/MeOH (1:1, v: v) to elute polar compounds. The concentration and compound specific carbon isotopic composition of pristane, phytane and aryl isoprenoids were analysed in the saturated and aromatic hydrocarbon fractions, respectively, and the original data reported in Tulipani et al. (in press), Jaraula et al. (2013) and Grice et al. (2005b). For the present study, the maleimide fractions were further processed following the protocol reported in Naeher et al. (2013). Each fraction was first purified by thin layer chromatography using 20% EtOAc in DCM as elutant and the band between retention factor 0.6 and 0.9 recovered. After derivatisation with MTBSTFA [N-(tert-butyldimethylsilyl)-N-methyl trifluoroacetamide, Sigma Aldrich] in pyridine (overnight at room temperature), the dried sample was eluted with DCM over a short silica gel column.

Maleimides were analysed by gas chromatography (GC) with an Agilent HP 6890 system equipped with an Agilent DB-5MS column [60 m x 0.25 mm inner diameter (i.d.) x 0.25 µm film thickness (f.t.)] with flame ionisation detector (FID). For identification and due to partly low concentrations, maleimides were also analysed by GC coupled to a mass spectrometer (GC-MS; Agilent 7890A coupled to Agilent 5975C inert XL EI/CI MSD) equipped with an identical column using electron impact ionisation (70 eV). The temperature program for both instruments was 40 °C (1 min isothermal), 40 °C to 100 °C at 10 °C min^{-1}, 100 °C to 320 °C at 4 °C min^{-1}, isothermal at 320 °C for 30 min. Helium was used as carrier gas (GC-FID: 2 mL min^{-1}; GC-MS: 1.2 mL min^{-1}).

For the MWR samples, Me,Et and Me,n-Pr maleimides were quantified by coinjection with the TBDMS derivative of phthalimide (ca. 4 ng/injection) on the

9

GC-FID. In contrast, Me,*n*-Pr maleimide concentration was too low in SAB samples and therefore quantified by GC-MS based on the peak area of the *m/z* 210 (base peak) mass chromatogram relative to the peak area of Me,Et maleimide in the *m/z* 75 mass chromatogram. Due to low concentration, Me,*i*-Bu maleimide was quantified by GC-MS based on the peak area of the *m/z* 224 (base peak) in all samples. For the PB samples the ratios of Me,Et maleimide and Me,*i*-Bu maleimide were calculated from base peaks of the maleimides by GC-MS analyses. Only relative concentrations are given as no response factors were determined for the quantification of maleimides.

3. Results and discussion

3.1. Reconstruction of redox conditions and photic zone euxinia by pristane/phytane ratios and aryl isoprenoid ratios

The Pr/Ph ratio is widely used to determine the redox conditions of the depositional environment, on the basis of the preferential formation of pristane and phytane from the phytyl side chain of chlorophyll *a* under oxic and anoxic conditions, respectively (Didyk et al., 1978; Peters et al., 2006). It was hypothesised that oxidation of phytol leads to the formation of pristane via the formation of a carboxylic group followed by decarboxylation, whereas phytane is formed by reduction of the hydroxyl group (e.g. Didyk et al., 1978). However, factors other than redox conditions may influence Pr/Ph ratios such as contributions from other sources (e.g. methanogenic and halophilic archaea),

10

and the tendency to increase with maturity of the samples (ten Haven et al., 1987; Peters et al., 2006).

The isoprenoids pristane and phytane were present in all samples from these cores (Grice et al., 2005a; 2005b; Jaraula et al., 2013; Tulipani et al., in press). The Pr/Ph ratios in the MWR samples were ≤ 1 in the lower unit and increased in the upper unit from 1 to 3 (Fig. 1a), which indicates a transition from reducing towards oxygenated conditions (Fig. 2) (Tulipani et al., in press). By contrast, the low Pr/Ph ratios ≤ 2 throughout the SAB profile (Fig. 1b) suggest anoxic conditions (Fig. 2) at time of deposition (Jaraula et al., 2013). In the studied PB section, Pr/Ph ratios decreased progressively from maximum values of 4 in the lowermost sample of the Permian part, with values ranging between 1 and 2 in the Triassic part of the core (Figs. 1c, 2), corresponding to a shift towards anoxia (Grice et al., 2005a; 2005b).

Tulipani et al. (in press) interpreted that the lower $\delta^{13}C$ values of phytane (-34 to -33 ‰) in the lower unit compared to the upper unit (-32 to -31 ‰; Fig. 1a) of the MWR core may reflect changing contributions of pristane and phytane from phytoplanktonic and bacterial sources, supported by similar $\delta^{13}C$ values of phytane and n-alkanes and significantly higher ratios of pristane/C_{17} n-alkane and phytane/C_{18} n-alkane in the lower unit. In contrast, $\delta^{13}C$ values of pristane and phytane were similar throughout the SAB profile, ranging mostly between -34 and -33 ‰, except a positive shift at 15 m with values of -30 and -29 ‰, respectively (Fig. 1b). Jaraula et al. (2013) tentatively interpreted this shift at the T/J boundary as relating to higher contributions from halophiles. This interpretation was based on the observation that the studied system

11

experienced a rise in sea level and a change towards a haline-mode circulation at the T/J boundary, which were driven by sinking warm brines (Kidder and Worsley, 2010). The higher salinity may have led to an increased abundance of halophilic archaea, which produce ^{13}C enriched isoprenoids relative to phytoplankton derived biomarkers (Grice et al., 1998; Jaraula et al., 2013). While most of the δ^{13}C values of pristane and phytane in the Triassic part of the PB profile ranged between -33 and -34 ‰, these values ranged between -38 and -26 ‰ in the Permian part (Fig. 1c). These up to 8‰ and 5‰ higher values for pristane and phytane, respectively (Fig. 1c), in the Upper Permian *vs.* the Lower Triassic section of the Hovea-3 core also indicate changing sources of pristane and phytane on the basis of δ^{13}C values in the PB dataset (Grice et al., 2005a; 2005b). These observations demonstrate that Pr/Ph ratios in all three sections may be partly biased by different sources and should therefore only be used in conjunction with other redox indicators for an unambiguous reconstruction of past redox conditions (ten Haven et al., 1987; Peters et al., 2006).

Aryl isoprenoids with 2,3,6-methylation patterns are suggestive of an origin from the carotenoid isorenieratene produced by Chlorobi, if occurring in a homologous series (Summons and Powell, 1987). In the SAB samples, all aryl isoprenoids between C_{13} and C_{22} were detected (Jaraula et al., 2013), whereas only the C_{13}–C_{21} aryl isoprenoids were present in the MWR samples (Tulipani et al., in press). The PB section contained a series of C_{12}–C_{31} aryl isoprenoids in the Griesbachian (Early Triassic) unit, whereas only traces of the C_{18} and C_{19} aryl isoprenoids could be detected in samples of the Changhsingian (Late

Permian) unit (Grice et al., 2005a; 2005b). However, only the concentrations of the C_{14}–C_{16} and C_{18}–C_{20} aryl isoprenoids were available for the PB section. Isorenieratane was detected through the T/J transition of the SAB profile, in the lower part of the MWR profile and in the upper unit of the PB profile, further indicating that aryl isoprenoids in the studied sections originate from Chlorobi (Grice et al., 2005a; 2005b; Jaraula et al., 2013; Tulipani et al., in press).

Stable carbon isotope values of aryl isoprenoids ranged between -21 and -15 ‰, and between -22 and -14 ‰, in the MWR and SAB sections, respectively (Jaraula et al., 2013; Tulipani et al., in press). These values were significantly higher than $\delta^{13}C$ signatures of n-alkanes and phytyl hydrocarbons, ranging between -34 and -28 ‰ in the MWR samples and between -38 and -29 ‰ in the SAB samples (Jaraula et al., 2013; Tulipani et al., in press). Therefore, the relative ^{13}C enrichment of at least 7 ‰ and up to 19 or 24 ‰ compared to n-alkanes and phytyl hydrocarbons in the MWR and SAB samples respectively, support a predominant origin from Chlorobi (Grice et al., 2005a; 2005b; Jaraula et al., 2013; Tulipani et al., in press). Due to low abundance, $\delta^{13}C$ values of aryl isoprenoids could not be determined in the PB samples (Grice et al., 2005a; 2005b).

Schwark and Frimmel (2004) demonstrated that the relationship of Pr/Ph *vs.* the aryl isoprenoid ratio (AIR), defined as (C_{13}–C_{17} 1-alkyl-2,3,6-trimethylbenzenes)/ (C_{18}–C_{22} 1-alkyl-2,3,6-trimethylbenzenes), can be used as a redox and PZE indicator and were also able to differentiate the changing degree of PZE throughout the studied Posidonia Black Shale profile. On the basis of detailed geological and sedimentological background information, the higher relative

13

abundance of the short-chain (C_{13}–C_{17}) aryl isoprenoids indicated a higher degree of oxic degradation of aryl isoprenoids, which was interpreted as more oxygenated conditions and therefore a lower degree of anoxic and euxinic conditions (Schwark and Frimmel, 2004).

In the geologic sections in the present study, AIR values were < 2 in the lower unit of the MWR profile and in the lowermost sample in the upper unit. In contrast, AIR values in the upper unit of MWR ranged from 3 to 7 (Fig. 1a). The low Pr/Ph ratios and the low AIR in the lower profile of MWR indicate reducing depositional conditions with more established PZE. In contrast to the MWR profile, AIR values were < 2 throughout the SAB profile except the uppermost and lowermost sample and in the upper PB section (lowest values at the P/T boundary), corresponding to low Pr/Ph ratios ≤ 2 (Figs. 1b, 1c). The low Pr/Ph ratios and low AIR values suggest reducing conditions and more established PZE close to the T/J and P/T boundaries in the SAB and PB profiles respectively (Figs. 1, 2). These interpretations are supported by the detection of isorenieratane in all sections (Grice et al., 2005a; 2005b; Jaraula et al., 2013; Tulipani et al., in press). There is debate as to whether changing redox conditions such as those seen in the studied formations can be attributed to changing intensity and periodicity of PZE, such as the distinction between episodic and persistent PZE proposed in Schwark and Frimmel (2004). Although higher AIR values may indicate more persistent PZE, low AIR values may also result from a persistent intermediate redox state or redox gradients.

The higher Pr/Ph ratios and higher AIR in the upper part of the MWR profile (Fig. 1a) corresponded to type III kerogen (HI values: 38-166; OI values: 32-200),

14

indicating a high input of terrestrial OM at times with more oxygenated conditions, which is supported by higher concentrations of methyltrimethyltridecylchromans (MTTCs) and perylene (Tulipani et al., in press). In contrast, relatively low carbon/nitrogen (6-18) and carbon/sulfur ratios (0-0.6) in the lower part of the profile and in the lowermost sample of the upper profile were associated with lower Pr/Ph ratios and lower AIR (Fig. 1a), which was interpreted as an open marine setting with persistent PZE and variably high terrestrial input (Tulipani et al., in press). Therefore, two clusters of samples representative of distinct changes in depositional conditions were dependent on the source of organic matter, as represented by the kerogen type in the MWR profile. In contrast to the MWR section, the low Pr/Ph ratios and low AIR values in the SAB profile (Figs. 1, 2) did not show a significant relation with the kerogen type, although lowest Pr/Ph values correspond to higher sea levels and less supply of terrestrial OM (Jaraula et al., 2013). In the PB section, the lower Pr/Ph ratios and AIR values in the Triassic part of the core (Fig. 1c) corresponded to a shift from a marine basin with high terrestrial input towards kerogen type II as a result of a marine transgression and associated persistent PZE (Grice et al., 2005a; 2005b). In contrast, the high Pr/Ph ratios in the Permian part of the core (Fig. 1c) indicated more oxidising conditions, despite the low AIR values (Figs. 1c, 2), which result from low concentrations or the absence of aryl isoprenoids in this section.

3.2. Maleimides as alternative indicators of photic zone euxinia

15

Maleimides were detected in all three sections and dominated by Me,Et maleimide, which can originate from most tetrapyrroles but is mainly derived from chlorophyll *a* and its derivatives (e.g. Grice et al., 1996; Naeher et al., 2013). Among other less abundant maleimides, Me,*n*-Pr maleimide and Me,*i*-Bu maleimide were present and originate from bacteriochlorophylls *c*, *d* and potentially also bacteriochlorophyll *e* after reduction of the aldehyde group in ring B based on structural grounds, which are derived from Chlorobi and can therefore indicate PZE depositional conditions (e.g. Grice et al., 1996; Naeher et al., 2013). Grice et al. (1996) suggested that the *n*-propyl group of Me,*n*-Pr maleimide may also be formed due to the reduction of the C_3 acid substituent of ring D in chlorophyll derivatives after ester hydrolysis. However, the strong positive correlation between Me,*i*-Bu maleimide and Me,*n*-Pr maleimide (R^2=0.98, n=11, p<0.01, MWR samples; R^2=0.99, n=7, p<0.01, SAB samples; Fig. 3) indicates either a common source from Chlorobi or that the source bacteria thrived under similar environmental conditions (e.g. Grice et al., 1996; Naeher et al., 2013).

The Me,*i*-Bu/Me,Et ratio was first used by Grice et al. (1997) as an approximate indicator of relative changes of PZE in ancient marine deposits, but has not been widely studied since. This indicator is based on changing bacteriochlorophyll to chlorophyll contributions due to changes in algal and bacterial biomass (Grice et al., 1997). Phototrophic sulfur bacteria thrive below phytoplankton communities within the water column or in deeper parts of microbial mats below benthic algae and cyanobacterial communities (Ormerod, 1983; Meyer et al., 2011; French et al., 2015). To adapt to the reduced light

intensities as a result of chlorophyll absorption, they produce bacteriochlorophylls with extended alkylations including *n*-propyl and *iso*-butyl groups to absorb light of longer wavelengths which is not absorbed by chlorophylls from algae and cyanobacteria (Ormerod, 1983; Rodrigo et al., 2000). Although benthic phototrophic sulfur bacteria may also be present, their impact cannot be investigated in palaeorecords due to the absence of diagnostic indicators to distinguish benthic and planktonic communities (Meyer et al., 2011; French et al., 2015).

High algal productivity can stimulate the development of anoxic and euxinic conditions due to the high oxygen demand of organic matter mineralisation within the water column and ultimately the photic zone (e.g. Meyer and Kump, 2008; Friedrich et al., 2014), associated with a relative increase in the Me,*i*-Bu/Me,Et and Me,*n*-Pr/Me,Et ratios. Other potential factors that favour PZE, leading to higher maleimide ratios, include higher thermal and salinity driven stratification stability, decreased oxygen solubility or basin restriction (e.g. Meyer and Kump, 2008). Therefore, higher Me,*i*-Bu/Me,Et and Me,*n*-Pr/Me,Et ratios may reflect more established PZE, consistent with observations in the Permian Kupferschiefer (Grice et al., 1997).

In the lower unit of the MWR profile, the Me,*i*-Bu/Me,Et and Me,*n*-Pr/Me,Et ratios decreased from 0.016 to 0.004, and from 0.037 to 0.041, respectively (Fig. 1a). In contrast, the ratios in the upper unit decreased first from maximum values of 0.010 and 0.023 at 33 m for Me,*i*-Bu/Me,Et and Me,*n*-Pr/Me,Et ratios, respectively, before increasing to almost the same values in the uppermost sample (Fig. 1a). The Me,*i*-Bu/Me,Et and Me,*n*-Pr/Me,Et ratios were moderately

to strongly, negatively correlated to AIR ratios in the lower unit of the MWR section with R^2 values of 0.82 and 0.96 (n=4; p<0.01), respectively, and in the upper unit with R^2 values of 0.55 and 0.56 (n=7; p<0.01), respectively (Figs. 4a, 4b).

In the SAB profile, the Me,i-Bu/Me,Et and Me,n-Pr/Me,Et ratios peaked at 15 m with values of 0.078 and 0.328, respectively (Fig. 1b). The same ratios were also moderately, negatively correlated to the AIR ratios with R^2 values of 0.74 and 0.59 (n=7; p<0.01), respectively (Figs. 4c, 4d).

At the P/T boundary in the PB profile, the Me,i-Bu/Me,Et ratio was highest with 0.59 (at 1981 m), with decreasing values in the Triassic part of the core (Fig. 1c). The maleimide data in the PB dataset were limited to Me,i-Bu/Me,Et ratios in the Triassic part of the profile (Grice et al., 2005a; 2005b), so there is no information available on the concentration of other maleimides or other maleimide ratios. In the PB dataset, the R^2 value between the Me,i-Bu/Me,Et ratio and the AIR was 0.59 (n=5; p<0.01; Fig. 4e).

The combination of all three datasets shows that Me,i-Bu/Me,Et and Me,n-Pr/Me,Et ratios increased up to 0.6 and 0.35, respectively, at AIR values below 2, whereas above AIR values of 2, both maleimide ratios remained low (<0.1; Figs. 4, 5). The moderate to strong, negative correlation of Me,i-Bu/Me,Et and Me,n-Pr/Me,Et ratios to the AIR in all data sets suggests that strongly reducing conditions accompanied by PZE are characterised by high values of the maleimide ratios and low AIR (Fig. 4). Therefore, the Me,i-Bu/Me,Et and Me,n-Pr/Me,Et ratios can be used as alternative indicators to reconstruct PZE in the geologic record.

Complications in the universal application of malemides as a proxy for PZE are demonstrated by a study from the Swiss Lake Rotsee (Naeher et al., 2013). This study showed that Me,*i*-Bu/Me,Et and Me,*n*-Pr/Me,Et ratios were higher prior to a strong increase in productivity and persistent PZE (Naeher et al., 2013). The decrease of Me,*i*-Bu maleimide and Me,*n*-Pr maleimide relative to Me,Et maleimide was explained by a community shift from Chlorobi to Chromatiaceae (Naeher et al., 2013). Higher productivity as a result of eutrophication may have led to a shallowing of the chemocline. This resulted in a larger biomass of Chromatiaceae, as indicated by the relative increase of okenone compared to isorenieratene (Züllig, 1985; Naeher et al., 2013). This community shift cannot be reconstructed on the basis of maleimides alone, as Chromatiaceae produce bacteriochlorophylls *a* and *b* without diagnostic alkylation patterns at ring B (e.g. Grice et al., 1996; Naeher et al., 2013). The higher abundance of Chromatiaceae, which thrive at shallower water depths than Chlorobi, may lead to a reduction of light penetration (Ormerod, 1983), thereby reducing the abundance of Chlorobi in this lake.

Chromatiaceae occur predominantly in shallow, stratified lakes (Pfennig and Trüper, 1981), which may limit the application of the proposed maleimide proxies in such systems. For the studied profiles in the present work, isorenieratane was detected and indicated the presence of Chlorobi (Grice et al., 2005a; 2005b; Jaraula et al., 2013; Tulipani et al., in press). However, okenone or its degraded counterpart okenane (Brocks and Schaeffer, 2008) could not be detected in the studied formations, suggesting that Chromatiaceae were most

likely absent, although it cannot be ruled out completely that Chromatiaceae were present which do not produce okenone.

The high values of both maleimide ratios and the low AIR in the lower profile of the MWR section, the upper profile in the PB section and in the middle of the SAB profile (Fig. 1) suggest that the Devonian, P/T and T/J mass extinction events were associated with persistent PZE, which agrees with previous interpretations (Grice et al., 2005a; 2005b; Jaraula et al., 2013; Tulipani et al., in press). The decrease in the maleimide ratios and the increase in the AIR in the MWR section may be related to a change from a restricted marine basin with enhanced stratification and PZE towards a vertically mixed marine water body (Tulipani et al., in press and references therein). In contrast, the change towards persistent PZE in the SAB section was explained by a rapid deepening of the shelf setting, followed by a return to episodic PZE (Jaraula et al., 2013). The PB section changed towards PZE as part of a marine transgression period due to climate change (Grice et al., 2005a; 2005b).

4. Conclusions

The Me,i-Bu/Me,Et and Me,n-Pr/Me,Et ratios in the studied sections reflect changing contributions from Chlorobi derived bacteriochlorophylls relative to chlorophylls and can be used as palaeoindicators of PZE, as indicated by the moderate to strong negative correlation to the carotenoid based AIR. These new proxies were applied successfully to reconstruct PZE in three geologic records that comprise three major mass extinction events. Our results suggest

that all three extinction events were characterised by persistent PZE. The maleimide ratios seem to be widely applicable for reconstructions of PZE in ancient and modern aquatic environments if the phototrophic sulfur bacterial community consists mainly of Chlorobi.

Acknowledgements

References

Barnosky, A.D., Matzke, N., Tomiya, S., Wogan, G.O.U., Swartz, B., Quental, T.B., Marshall, C., McGuire, J.L., Lindsey, E.L., Maguire, K.C., Mersey, B., Ferrer, E.A., 2011. Has the Earth's sixth mass extinction already arrived? Nature 471, 51-57.

Becker, R.T., House, M.R., Kirchgasser, W.T., Playford, P.E., 1991. Sedimentary and faunal changes across the frasnian/famennian

boundary in the canning basin of Western Australia. Historical Biology 5, 183-196.

Brocks, J.J., Summons, R.E., 2003. Sedimentary hydrocarbons, biomarkers for early life. In: Holland, H.D., Turekian, K. (Eds.), Treatise in Geochemistry. Elsevier, Oxford, pp. 65-115.

Brocks, J.J., Love, G.D., Summons, R.E., Knoll, A.H., Logan, G.A., Bowden, S.A., 2005. Biomarker evidence for green and purple sulphur bacteria in a stratified Palaeoproterozoic sea. Nature 437, 866-870.

Brocks, J.J., Schaeffer, P., 2008. Okenane, a biomarker for purple sulfur bacteria (Chromatiaceae), and other new carotenoid derivatives from the 1640 Ma Barney Creek Formation. Geochimica et Cosmochimica Acta 72, 1396-1414.

Cao, C., Love, G.D., Hays, L.E., Wang, W., Shen, S., Summons, R.E., 2009. Biogeochemical evidence for euxinic oceans and ecological disturbance presaging the end-Permian mass extinction event. Earth and Planetary Science Letters 281, 188-201.

Diaz, R.J., Rosenberg, R., 2008. Spreading dead zones and consequences for marine ecosystems. Science 321, 926-929.

Didyk, B.M., Simoneit, B.R.T., Brassell, S.C., Eglinton, G., 1978. Organic geochemical indicators of palaeoenvironmental conditions of sedimentation. Nature 272, 216-222.

French, K.L., Rocher, D., Zumberge, J.E., Summons, R.E., 2015. Assessing the distribution of sedimentary C_{40} carotenoids through time. Geobiology 13, 139-151.

Friedrich, J., Janssen, F., Aleynik, D., Bange, H.W., Boltacheva, N., Çagatay, M.N., Dale, A.W., Etiope, G., Erdem, Z., Geraga, M., Gilli, A., Gomoiu, M.T., Hall, P.O.J., Hansson, D., He, Y., Holtappels, M., Kirf, M.K., Kononets, M., Konovalov, S., Lichtschlag, A., Livingstone, D.M., Marinaro, G., Mazlumyan, S., Naeher, S., North, R.P., Papatheodorou, G., Pfannkuche, O., Prien, R., Rehder, G., Schubert, C.J., Soltwedel, T., Sommer, S., Stahl, H., Stanev, E.V., Teaca, A., Tengberg, A., Waldmann, C., Wehrli, B., Wenzhöfer, F., 2014. Investigating hypoxia in aquatic environments: diverse approaches to addressing a complex phenomenon. Biogeosciences 11, 1215-1259.

Grice, K., Gibbison, R., Atkinson, J.E., Schwark, L., Eckardt, C.B., Maxwell, J.R., 1996. Maleimides (1H-pyrrole-2,5-diones) as molecular indicators of anoxygenic photosynthesis in ancient water columns. Geochimica et Cosmochimica Acta 60, 3913-3924.

Grice, K., Schaeffer, P., Schwark, L., Maxwell, J.R., 1997. Changes in palaeoenvironmental conditions during deposition of the Permian Kupferschiefer (Lower Rhine Basin, northwest Germany) inferred from molecular and isotopic compositions of biomarker components. Organic Geochemistry 26, 677-690.

Grice, K., Schouten, S., Nissenbaum, A., Charrach, J., Sinninghe Damsté, J.S., 1998. Isotopically heavy carbon in the C_{21} to C_{25} regular isoprenoids in halite-rich deposits from the Sdom Formation, Dead Sea Basin, Israel. Organic Geochemistry 28, 349-359.

Grice, K., Cao, C., Love, G.D., Böttcher, M.E., Twitchett, R.J., Grosjean, E., Summons, R.E., Turgeon, S.C., Dunning, W., Jin, Y., 2005a. Photic zone euxinia during the Permian-Triassic superanoxic event. Science 307, 706-709.

Grice, K., Summons, R.E., Grosjean, E., Twitchett, R.J., Dunning, W.J., Wang, S., Bottcher, M.E., 2005b. Depositional conditions of the Northern onshore Perth basin (Basal Triassic). Australian Petroleum Production and Exploration Association Journal 1, 263-273.

Grice, K., Twitchett, R.J., Alexander, R., Foster, C.B., Looy, C., 2005c. A potential biomarker for the Permian–Triassic ecological crisis. Earth and Planetary Science Letters 236, 315-321.

Hallam, A., Wignall, P.B., 1997. Mass Extinctions and Their Aftermath. Oxford University Press, UK.

Hesselbo, S.P., Robinson, S.A., Surlyk, F., 2004. Sea-level change and facies development across potential Triassic-Jurassic boundary horizons, SW Britain. Journal of the Geological Society 161, 365-379.

Hounslow, M.W., Posen, P.E., Warrington, G., 2004. Magnetostratigraphy and biostratigraphy of the Upper Triassic and lowermost Jurassic succession, St. Audrie's Bay, UK. Palaeogeography, Palaeoclimatology, Palaeoecology 213, 331-358.

Jaraula, C.M.B., Grice, K., Twitchett, R.J., Böttcher, M.E., LeMetayer, P., Dastidar, A.G., Opazo, L.F., 2013. Elevated pCO_2 leading to Late Triassic extinction, persistent photic zone euxinia, and rising sea levels. Geology 41, 955-958.

Kidder, D.L., Worsley, T.R., 2010. Phanerozoic Large Igneous Provinces (LIPs), HEATT (Haline Euxinic Acidic Thermal Transgression) episodes, and mass extinctions. Palaeogeography, Palaeoclimatology, Palaeoecology 295, 162-191.

Koopmans, M.P., Koster, J., van Kaam-Peters, H.M.E., Kenig, F., Schouten, S., Hartgers, W.A., de Leeuw, J.W., Sinninghe Damsté, J.S., 1996. Diagenetic and catagenetic products of isorenieratene: Molecular indicators for photic zone anoxia. Geochimica et Cosmochimica Acta 60, 4467-4496.

Lyons, T.W., Anbar, A.D., Severmann, S., Scott, C., Gill, B.C., 2009. Tracking Euxinia in the Ancient Ocean: A Multiproxy Perspective and Proterozoic Case Study. Annual Review of Earth and Planetary Sciences 37, 507-534.

Mander, L., Twitchett, R.J., Benton, M.J., 2008. Palaeoecology of the Late Triassic extinction event in the SW UK. Journal of the Geological Society 165, 319-332.

Meyer, K.M., Kump, L.R., 2008. Oceanic euxinia in Earth history: causes and consequences. Annual Review of Earth and Planetary Sciences 36, 251-288.

Meyer, K.M., Macalady, J.L., Fulton, J.M., Kump, L.R., Schaperdoth, I., Freeman, K.H., 2011. Carotenoid biomarkers as an imperfect reflection of the anoxygenic phototrophic community in meromictic Fayetteville Green Lake. Geobiology 9, 321-329.

Middelburg, J.J., Levin, L.A., 2009. Coastal hypoxia and sediment biogeochemistry. Biogeosciences 6, 1273-1293.

Nabbefeld, B., Grice, K., Twitchett, R.J., Summons, R.E., Hays, L., Böttcher, M.E., Asif, M., 2010. An integrated biomarker, isotopic and palaeoenvironmental study through the Late Permian event at Lusitaniadalen, Spitsbergen. Earth and Planetary Science Letters 291, 84-96.

Naeher, S., Schaeffer, P., Adam, P., Schubert, C.J., 2013. Maleimides in recent sediments – Using chlorophyll degradation products for palaeoenvironmental reconstructions. Geochimica et Cosmochimica Acta 119, 248-263.

Ormerod, J.G., 1983. The Phototrophic bacteria: anaerobic life in the light. Blackwell Science Ltd.

Peters, K.E., Walters, C.C., Moldowan, J.M., 2006. The Biomarker Guide: II. Biomarkers and Isotopes in Petroleum Exploration and Earth History. Cambridge University Press, Cambridge, UK.

Pfennig, N., 1978. General physiology and ecology of photosynthetic bacteria. In: Clayton, R.K., Sistrom, W.R. (Eds.), Photosynthetic Bacteria. Plenum Press, pp. 3-16.

Pfennig, N., Trüper, H.G., 1981. Isolation of members of the families Chromatiaceae and Chlorobiaceae. In: Starr, M.P., Trüper, H.G., Balows, A., Schlegel, H.G. (Eds.), The prokaryotes. Springer, pp. 279–289.

Playford, P.E., Hocking, R.M., Cockbain, A.E., 2009. Devonian reef complexes of the Canning Basin, Western Australia, Geological Survey of Western Australia Bulletin 145, 444p.

Raup, D.M., Sepkoski, J.J., 1982. Mass extinctions in the marine fossil record. Science 215, 1501-1503.

Rodrigo, M.A., Vicente, E., Miracle, M.R., 2000. The role of light and concentration gradients in the vertical stratification and seasonal development of phototrophic bacteria in a meromictic lake. Archives of Hydrobiology 148, 533–548.

Schwark, L., Frimmel, A., 2004. Chemostratigraphy of the Posidonia Black Shale, SW-Germany: II. Assessment of extent and persistence of photic-zone anoxia using aryl isoprenoid distributions. Chemical Geology 206, 231-248.

Summons, R.E., Powell, T.G., 1987. Identification of aryl isoprenoids in source rocks and crude oils: Biological markers for the green sulphur bacteria. Geochimica et Cosmochimica Acta 51, 557-566.

ten Haven, H.L., de Leeuw, J.W., Rullkotter, J., Sinninghe Damsté, J.S., 1987. Restricted utility of the pristane/phytane ratio as a palaeoenvironmental indicator. Nature 330, 641-643.

Thomas, B.M., Willink, R.J., Grice, K., Twitchett, R.J., Purcell, R.R., Archbold, N.W., George, A.D., Tye, S., Alexander, R., Foster, C.B., Barber, C.J., 2004. Unique marine Permian–Triassic boundary section from Western Australia. Australian Journal of Earth Sciences 51, 423-430.

Tulipani, S., Grice, K., Greenwood, P.F., Haines, P., Sauer, P., Schimmelmann, A., Summons, R.E., Foster, A.E., Böttcher, M.E., Playton, T., Schwark, L., in press. Changes in palaeoenvironmental conditions in Late Devonian Reef systems from the Canning Basin, WA: A biomarker and stable isotope approach. Gondwana Research. doi:10.1016/j.gr.2014.10.003.

Twitchett, R.J., 2006. The palaeoclimatology, palaeoecology and palaeoenvironmental analysis of mass extinction events. Palaeogeography, Palaeoclimatology, Palaeoecology 232, 190-213.

Züllig, H., 1985. Carotenoids from plankton and purple sulfur bacteria in lake sediments as indicators of changes in the environment. Experientia 41, 533-534.

Figure captions

Fig. 1. Simplified stratigraphy and ages of studied formations together with profiles of Pristane/Phytane (Pr/Ph) ratios, δ^{13}C values of pristane and phytane, aryl isoprenoid datios (AIR), Me,i-Bu/Me,Et ratios and Me,n-Pr/Me,Et ratios of the a) McWhae Ridge (MWR), b) St. Audrie's Bay (SAB) and c) Perth Basin (PB) datasets. Pr/Ph ratios, δ^{13}C values of pristane and phytane and AIR data from the MWR, SAB and PB samples were adapted from Tulipani et al. (in press), Jaraula et al. (2013) and Grice et al. (2005a; 2005b), respectively. Stratigraphy and ages of the MWR, SAB and PB sections were adapted from Tulipani et al. (in press), Jaraula et al. (2013) and Thomas et al. (2004).

Fig. 2. Plots of Pristane/Phytane (Pr/Ph) ratios *vs.* aryl isoprenoid ratios (AIR) for all studied sections. Arrows indicate oxidising *vs.* reducing conditions and photic zone euxinia (PZE). The data from the McWhae Ridge (MWR), St. Audrie's Bay (SAB) and Perth Basin (PB) samples were adapted from Tulipani et al. (in press), Jaraula et al. (2013) and Grice et al. (2005a; 2005b), respectively.

Fig. 3. Correlation between concentrations of Me,*i*-Bu maleimide *vs.* Me,*n*-Pr maleimides in datasets from a) McWhae Ridge (MWR) and b) St. Audrie's Bay (SAB) with correlation coefficient (R^2) values.

Fig. 4. Correlation between the Me,*i*-Bu/Me,Et ratios *vs.* AIR (left) and Me,*n*-Pr/Me,Et ratios *vs.* AIR (right) with correlation coefficient (R^2) values for a/b) upper and lower units of McWhae Ridge samples (MWR), c/d) St. Audrie's Bay (SAB) and e/f) Perth Basin (PB). The AIR data from the MWR, SAB and PB samples were adapted from Tulipani et al. (in press), Jaraula et al. (2013) and Grice et al. (2005a; 2005b), respectively.

Fig. 5. Combined dataset of a/c) Me,*i*-Bu/Me,Et ratios *vs.* AIR and b/d) Me,*n*-Pr/Me,Et ratios *vs.* AIR comprising all samples from McWhae Ridge (MWR), St. Audrie's Bay (SAB) and Perth Basin (PB). While a) and b) show the rise in maleimide values at AIR below 2, whereas c) and d)

show the same dataset plotted on a logarithmic scale of the y-axis to show the variation in the datasets with low ratios. The AIR data from the MWR, SAB and PB samples were adapted from Tulipani et al. (in press), Jaraula et al. (2013) and Grice et al. (2005a; 2005b), respectively.
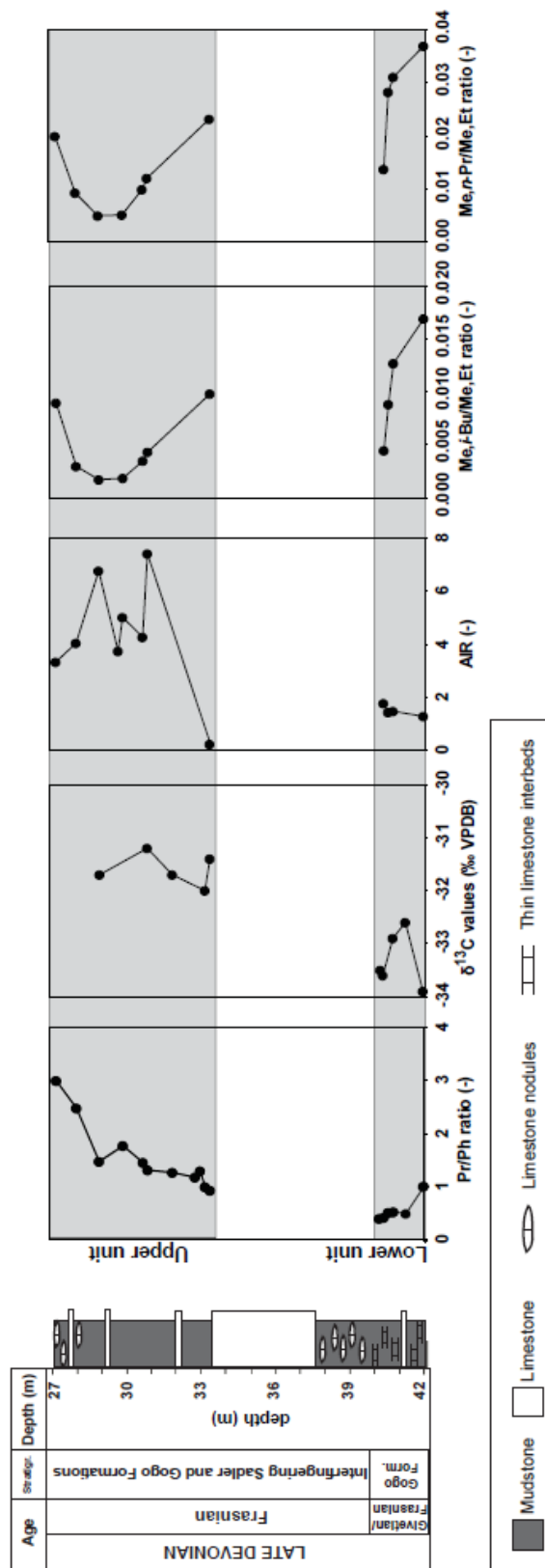
Figure 1a

Figure 1b

Figure 1c

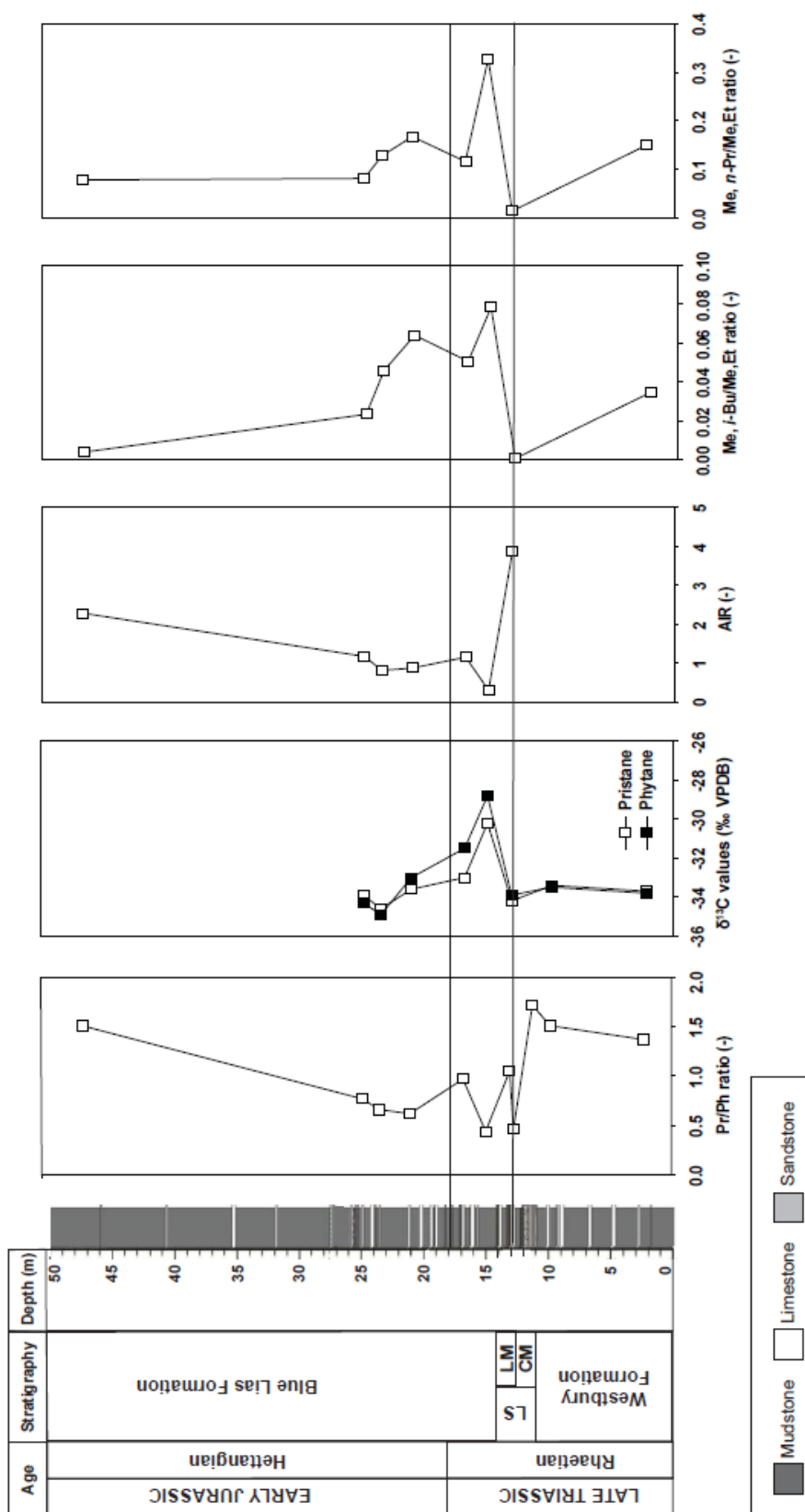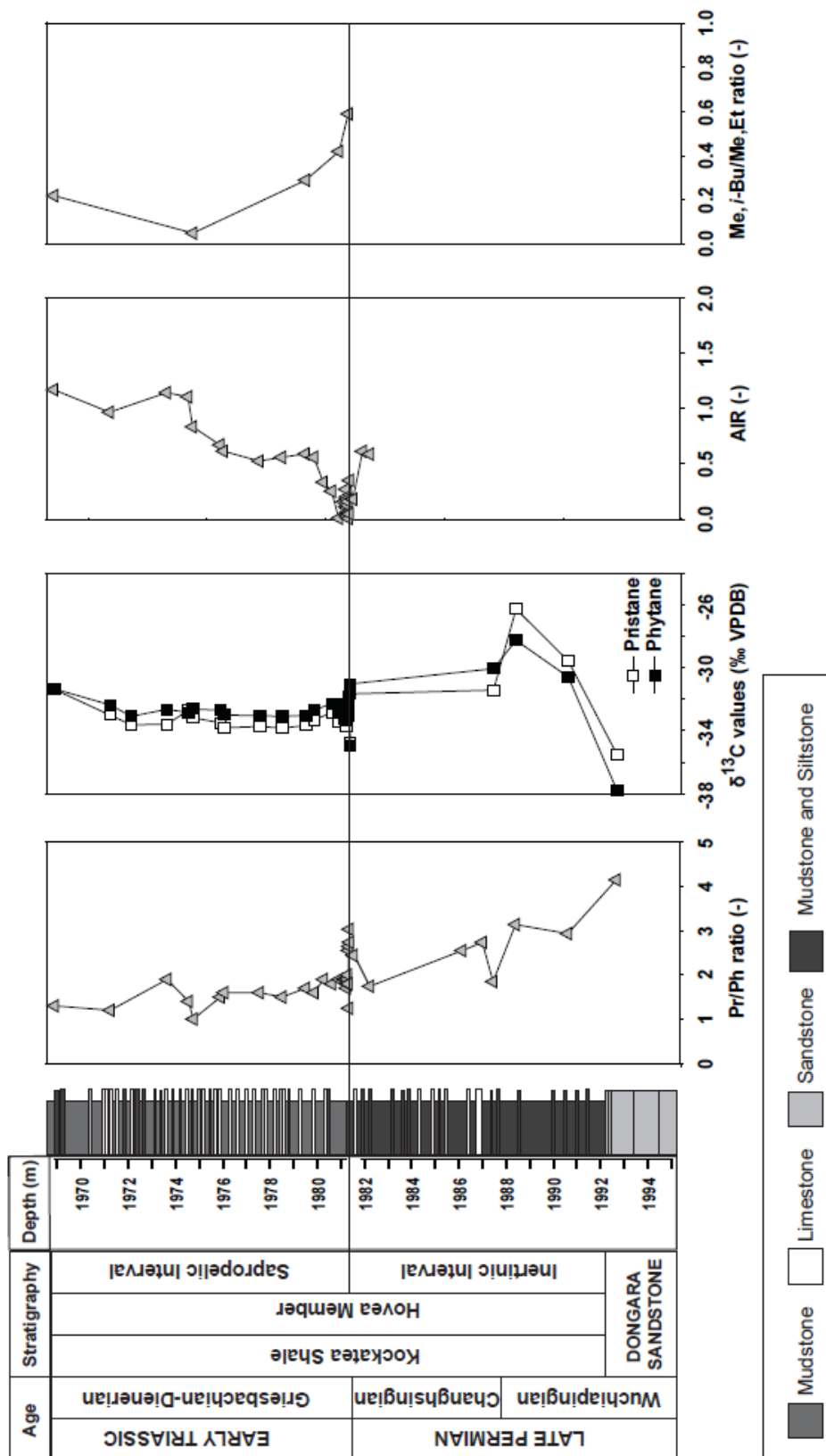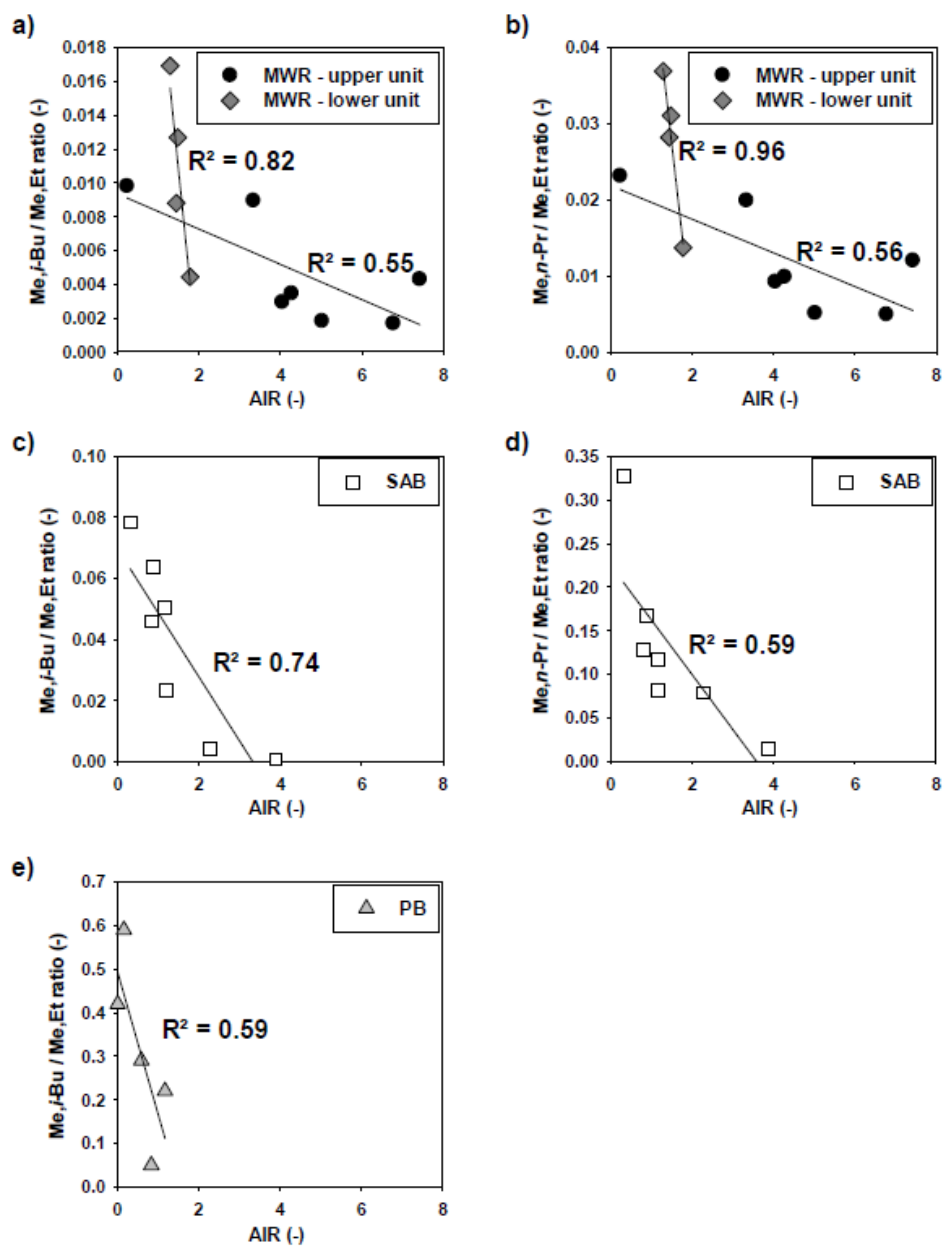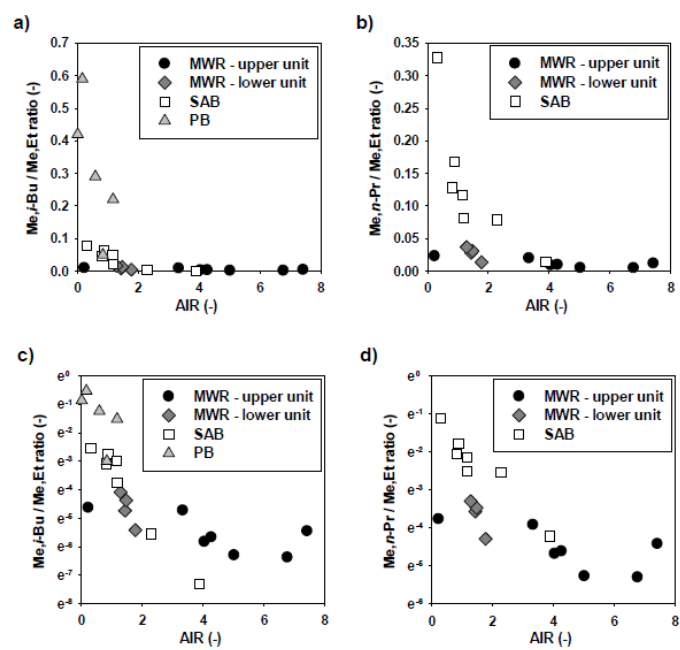**Figure 2**

Figure 3

a)

b)
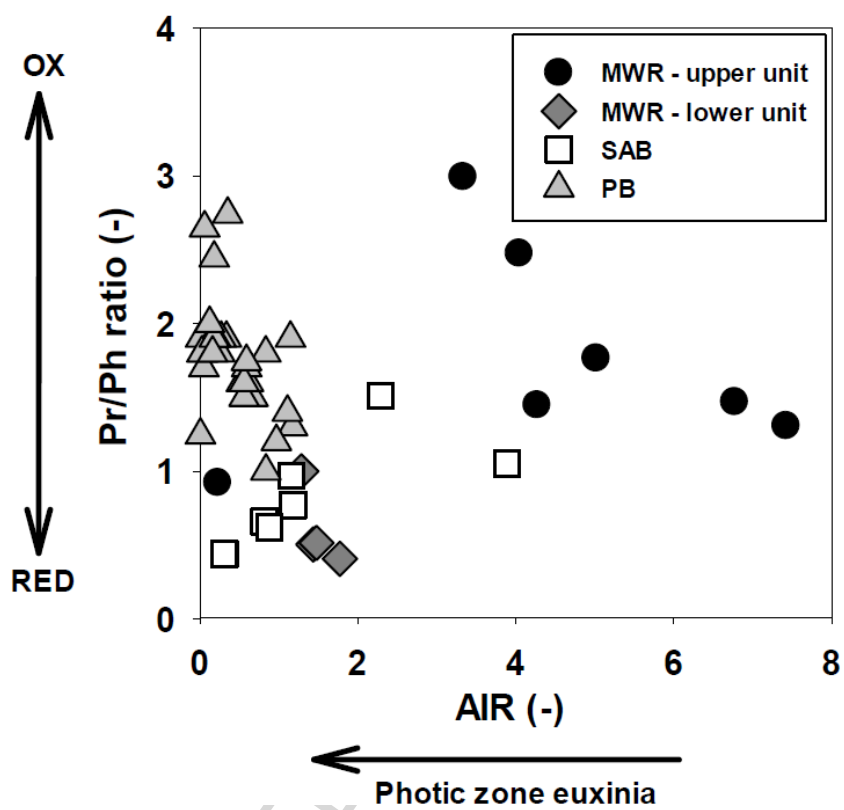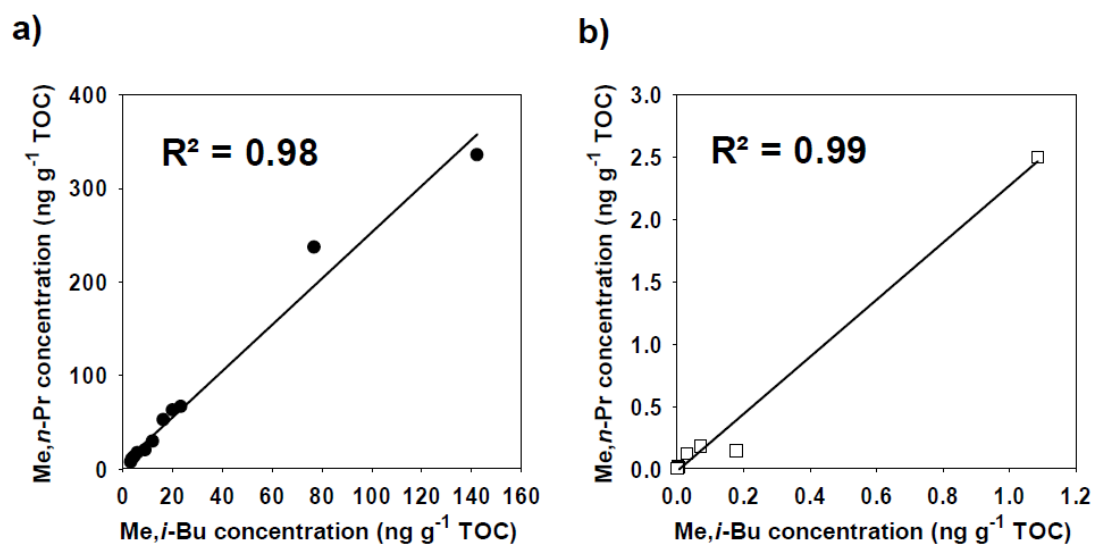
Figure 4

Figure 5

Manuscript highlights:

- Pristane/phytane ratios and aryl isoprenoid ratios used as indicators of ancient redox conditions and photic zone euxinia

- Maleimide ratios proposed as new, robust indicators of photic zone euxinia

- All three mass extinction events were affected by persistent photic zone euxinic depositional conditions